Journal of Volcanology and Geothermal Research 320 (2016) 117–127

Contents lists available at ScienceDirect

Journal of Volcanology and Geothermal Research

journal homepage: www.elsevier.com/locate/jvolgeores

Time-scale and mechanism of subsidence at Lassen Volcanic Center, CA, from InSAR

Amy L. Parker [a,*,1,2], Juliet Biggs [a,1], Zhong Lu [b]

[a] School of Earth Sciences, University of Bristol, Bristol, UK
[b] Roy M. Huffington Department of Earth Sciences, Southern Methodist University, Dallas, TX, United States

ARTICLE INFO

Article history:
Received 2 November 2015
Received in revised form 1 April 2016
Accepted 11 April 2016
Available online 16 April 2016

ABSTRACT

Observations of volcanic subsidence have contributed to our understanding of the eruption cycle, hydrothermal systems and the formation of continental crust. Lassen Volcanic Center is one of two volcanoes in the southern Cascades known to have subsided in recent decades, but the onset, temporal evolution, and cause of subsidence remain unconstrained. Here we use multiple sets of InSAR data, each corrected using the North American Regional Reanalysis atmospheric model, to determine the temporal and spatial characteristics of deformation between 1992 and 2010. Throughout this period all datasets reveal subsidence of a broad, 30–40 km wide region at rates of ~10 mm/yr. Evaluating past geodetic studies we suggest that subsidence may have been ongoing since the 1980s, before which it is unlikely that significant ground deformation occurred. By combining multiple tracks of InSAR data we find that the ratio of horizontal to vertical displacements is high (up to 3:1), and source inversions favour a point source located at ~8 km depth. Time-series analysis suggests that the rate of volume change of this source may have varied over time. The source geometry and the temporal evolution of deformation contrasts to subsidence observed at nearby Medicine Lake Volcano since the 1950s. We evaluate possible causes of subsidence at Lassen Volcanic Center in light of tectonic setting and hydrothermal activity, and suggest that regional GPS measurements will be key to understanding the role of crustal extension plus other hydrothermal/magmatic processes in deformation during recent decades.

1. Introduction

Observing and understanding ground deformation at volcanoes provides insight into the dynamics of the magmatic and/or hydrothermal system (see Pinel et al., 2014 and references therein). InSAR observations alone document ground displacements at >500 volcanoes worldwide (Biggs et al., 2014). These studies identify ground deformation such as: transient subsidence linked to co-eruptive volume loss (e.g., Okmok Volcano, Aleutians: Lu et al., 1998); cyclical bradyseisms, associated with the interaction between magmatic fluids and hydrothermal systems (e.g., Campi Flegrei, Italy: Chiodini et al., 2015); and long wavelength, steady uplift, related to heat transfer and crustal ductility induced by deep magma bodies (e.g., Sorocco, New Mexico: Pearse and Fialko, 2010).

Lassen Volcanic Center (LVC) is the southernmost volcano of the Cascades Volcanic Arc (Fig. 1A) and the only Cascade volcano other than Mount St. Helens to have erupted during the 20th century (Clynne et al., 2012). LVC is also one of two volcanic centers in northern California known to be subsiding (Dzurisin et al., 1991; Poland et al., 2004), although whether this is associated with the eruption (e.g., withdrawal of magmatic fluids), the vigorous hydrothermal system, or regional tectonics, is undetermined (Poland et al., 2004). Constraining the onset, rate, and spatial characteristics of subsidence at LVC is therefore key to understanding the behavior of the volcano. This has implications for hazard assessments, as LVC is located within a National Park, and lies in the path of major air traffic corridors, gas pipelines and power lines (Clynne et al., 2012).

Geodetic surveys of LVC prior to 1996 consisted of leveling (1932, 1934, 1991: Dzurisin, 1999), repeated electronic distance measurements (EDM) and dry tilt surveys (1981, 1982, 1984: Chadwick et al., 1985), all of which showed no conclusive evidence of ground deformation (Fig. 1B). However, an InSAR survey of the volcano in 1996–2000 indicated up to ~10 mm/yr of subsidence over a ~40 km diameter area centered 5 km SE of Lassen Peak (Poland et al., 2004). This motivated a survey of 5 EDM lines using GPS in 2004, which revealed that line lengths had shortened by up to 145 mm since 1981 (Poland et al., 2004). Here we consolidate past geodetic measurements at LVC with a detailed InSAR survey between 1992 and 2010 to constrain the spatial and temporal evolution of ground deformation. Using these results, we evaluate possible mechanisms of subsidence, and also draw

* Corresponding author: Dr. Amy L. Department of Spatial Sciences, Curtin University, Perth Australia. Phone: +61426052221.
E-mail address: Amy.Parker@curtin.edu.au (A.L. Parker).
[1] COMET (Centre for the Observation and Modelling of Earthquakes, Volcanoes and Tectonics).
[2] Now at: The Institute of Geoscience Research and Department of Spatial Sciences, Curtin University, Perth, Western Australia, Australia.

http://dx.doi.org/10.1016/j.jvolgeores.2016.04.013
0377-0273/

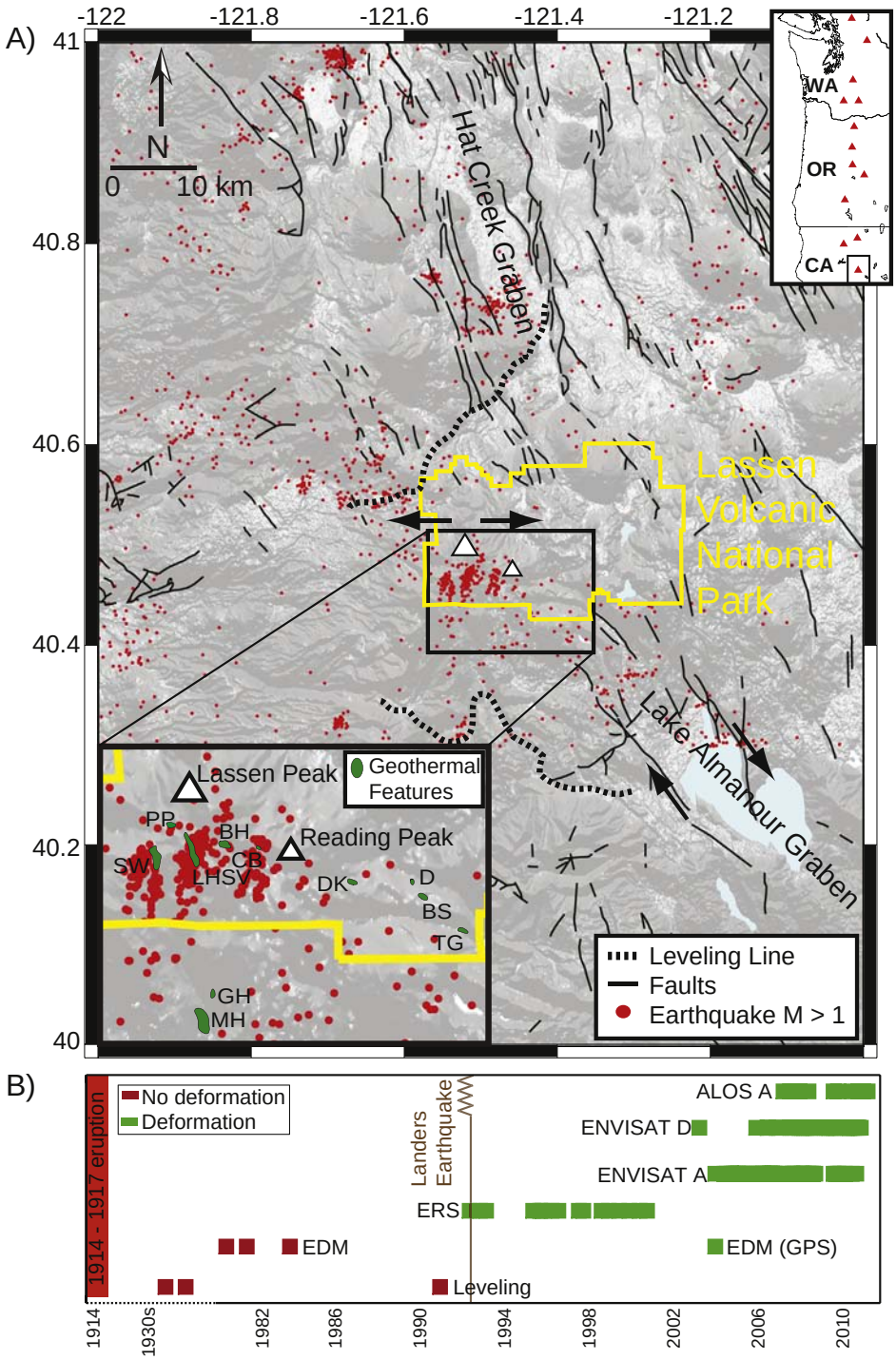

Fig. 1. A) Map of LVC including main regional structural features after Clynne and Muffler (2010) and earthquake locations (2000–2014) from the Northern California Earthquake Data Center. Solid arrows show the direction of E–W extension across LVC and dextral shear SE of Devil's Kitchen (DK) (Janik and McLaren, 2010). The leveling lines are from Dzurisin (1999). Top inset: map shows the location of LVC in the Cascades Volcanic Arc. Bottom inset: clusters of seismicity and hydrothermal features. LHSV — Little Hot Springs Valley, BH — Bumpass Hell, SW — Sulphur Works, PP — Pilot Pinnacle solfataras, DK — Devil's Kitchen, GH — Growler Hot Springs and MH — Morgan Hot Springs. B) Time-line summarising the acquisition of geodetic data at LVC (Leveling: Dzurisin, 1999; EDM: Chadwick et al., 1985; GPS: Poland et al., 2004). Red corresponds to surveys that did not show deformation and green corresponds to surveys that show subsidence. The date of the 1992 Landers earthquake is shown for reference. (For interpretation of the references to colour in this figure legend, the reader is referred to the web version of this article.)

comparisons with deformation recorded at Medicine Lake Volcano located 100 km to the north.

1.1. Tectonic and geological setting

The Lassen region marks the southern end of the Cascades Volcanic Arc (Fig. 1A) and the interaction between subduction along the Cascadia subduction zone and extension of the Basin and Range province (e.g., Wells et al., 1998; Hildreth, 2007). N and S of Lassen Volcanic National Park are the Hat Creek and Lake Almanor Grabens respectively (Fig. 1A), which are the westernmost structures of the Basin and Range in this region (Clynne and Muffler, 2010). LVC is also coincident with a transitional zone of the Walker Lane fault system, where horizontal stress is transferred from NW dextral shear in the SE to E–W

extension in the N (Janik and McLaren, 2010). Accordingly, motion on regional faults is seen to have a strike–slip component (e.g., Blakeslee and Kattenhorn, 2013). In addition to faulting, NNW trending breaks between Lassen Peak and Reading Peak have been described as a zone of tensional surface deformation, possibly related to a near-surface dike emplaced just prior to the 1914 eruption (Clynne and Muffler, 2010).

Volcanism in the Lassen region has been ongoing for ~3 Ma (Clynne and Muffler, 2010). The current manifestation of LVC began ~825 ka with the formation of the Rockland caldera complex, and during the last 1100 years, three eruptions have occurred including the 1914–1917 eruption at Lassen Peak (Clynne and Muffler, 2010). This eruption was associated with an erupted volume of ~0.025 km^3 (Clynne et al., 2012), comprised of a dacite dome and lava flow, dacite pyroclastic flow, plus phreatic, avalanche, debris-flow, flood and fall deposits (Clynne and Muffler, 2010), resulting in what is now known as the Devastated Area within Lassen Volcanic National Park.

The LVC magmatic system has been interpreted to contain one or more small dispersed magma bodies in a larger, but mostly solidified zone of silicic magma (Clynne, 1985). This is comparable to the magmatic model proposed for neighbouring Medicine Lake Volcano (Dzurisin et al., 2002; Donnelly-Nolan et al., 2008), and is in agreement with seismic surveys that detect low-velocity zones in the crust, but do not identify a discrete magma reservoir larger than the detection limit (5 km diameter) (Clynne, 1985). Most recent evidence suggests that LVC silicic magmas are derived from pressures of ~145 MPa, equivalent to ~5 km depth (Quinn, 2014), and that the area of young volcanism is underlain by a zone of crystal mush that is too viscous to erupt (Klemetti and Clynne, 2014). Zircon age analysis provides evidence of mush rejuvenation (and remobilisation) by basaltic intrusions on timescales of 10s–1000s years, facilitating eruptions of magma from within this otherwise cooling magmatic body (Klemetti and Clynne, 2014).

1.2. Hydrothermal and seismic activity

Hydrothermal activity at LVC is vigorous, with steam vents, fumaroles, hot springs, and extensive alteration of surface rocks that has resulted in numerous landslides (Clynne et al., 2012). Geochemical and seismic analysis suggest that there are two separate hydrothermal cells at ~5 km depth that circulate within the greater Lassen hydrothermal system (Janik and McLaren, 2010). One cell feeds steam to Little Hot Springs Valley, Bumpass Hell, Sulphur Works and Pilot Pinnacle solfataras (LHSV, BH, SW and PP in Fig. 1A), and the second cell beneath the Devil's Kitchen area (DK in Fig. 1A) is recharged by precipitation that percolates via permeable faults of the Walker Lane (Janik and McLaren, 2010).

LVC is also one of the most seismically active Cascade volcanoes, with the majority of events occurring at depths <7 km in three N–S elongate zones (the West, Middle and East clusters) (Humphrey and McLaren, 1995) (Fig. 1A). Overall approximately 25% of events are attributed to the hydrothermal system (Klein, 1979; Walter et al., 1984), and the base of the hydrothermal system is thought to be coincident with a zone of persistent seismicity at 4–5 km depth (Ingebritsen et al., 2016). Seismicity in the East cluster is also the result of motion along faults of the Walker Lane (McLaren and Janik, 1996), and deeper events (7–10 km depth) that occur beneath Devil's Kitchen (DK Fig. 1A) correlate with local fault orientations. Three vigorous earthquake sequences, with events up to M_w 5.5, occurred in 1936, 1945–1947, and 1950, and were attributed to approximately E-W extension localized on Basin and Range normal faults at the southern boundary of Lassen Volcanic National Park (Norris et al., 1997). The most recent earthquake swarm in November 2014 is attributed to upward migration of hydrothermal fluids, and includes a M_w 3.85 earthquake, the largest event within 30 km of Lassen Peak in >60 years (Ingebritsen et al., 2015). Changes in permeability induced by this event are thought to have caused a two-fold increase in hydrothermal outflow from a localized hydrothermal aquifer at Growler/Morgan Hot Springs (GH and MH in Fig. 1A) (Ingebritsen et al., 2015). Long period (LP) earthquakes (associated with the movement of magma at depth and magmatic/hydrothermal interactions) are also common at LVC. These events typically occur in clusters in a region 5–8 km west of Lassen Peak at depths of 13–23 km (Pitt et al., 2002). Between 2003 and 2011 an average of 11 LP earthquakes were detected per year (A.M. Pitt, unpublished data in Clynne et al., 2012).

2. Methods

2.1. InSAR data and processing

We investigate subsidence at LVC using 4 sets of InSAR data spanning 1992–2010 (Table 1; Fig. 1B). The first dataset is from European Space Agency C-band satellite ERS-1/2 descending track 70, and includes the scenes used by Poland et al. (2004). In total we successfully form 55 ERS-1/2 interferograms spanning summer (snow-free) months between 1992 and 2000. We also use imagery from the European Space Agency C-band satellite ENVISAT ascending track 435 (82 interferograms) and descending track 342 (104 interferograms), spanning 2004–2010, plus imagery from the JAXA satellite ALOS ascending track 163 (16 interferograms) covering 2007–2010. All interferograms were processed using JPL/Caltech software ROI_PAC (Rosen et al., 2004), filtered using a power spectrum filter (Goldstein and Werner, 1998), unwrapped using a branch-cut algorithm at 16 looks (Goldstein et al., 1988) and down-sampled to a final resolution of ~300 m (e.g., Jónsson et al., 2002). Orbital errors were removed using linear ramps (Biggs et al., 2007; Gourmelen et al., 2010), and topographically-correlated atmospheric artifacts were reduced using the North American Regional Reanalysis atmospheric model as described in Parker et al. (2015). Interferograms were processed and analyzed in the original frames and then cropped to the overlapping region. Multi temporal analysis was then used to combine information from many interferograms, increasing the signal to noise ratio of the datasets and allowing us to investigate the evolution of deformation over time.

2.2. Stacking

Visual inspection of interferograms reveals that the deformation signal is spatially consistent over the observation period. We therefore use stacking to first investigate the location and spatial extent of subsidence. Interferograms were selected for stacking based upon the criteria described by Parker et al. (2014), whereby analysis of the coherence and noise properties of each dataset are used to set selection thresholds (Fig. 2). For the ENVISAT and ALOS datasets we select interferograms that have >80% of pixels above the coherence threshold used in processing and σ <15 mm, where σ is interferogram standard deviation calculated using covariance analysis (Hanssen, 2001). We use lower thresholds of σ <5 mm, and coherence >30% for ERS - 1/2 as we find that 70% of interferograms in this dataset are <50% coherent (Fig. 2A). The resulting data subsets (Table 1) contain 36 ERS-1/2 descending track interfergrams (June 1992–September 2000); 25 ENVISAT ascending track interferograms (August 2004–August 2010); 34 ENVISAT descending track interferograms (July 2007–September 2010); and 9 ascending track ALOS interferograms (September 2007–November 2010). Stacks were then produced for all pixels that are coherent in >2 interferograms by summing together the displacements from all interferograms coherent at each pixel, and dividing by the total duration of the constituent interferograms. Measurements were then referenced to a far-field, non-deforming region.

Using the results of stacking, we solve for the horizontal (eastward) and vertical components of the deformation field, $\mathbf{u} = (u_E, u_Z)^T$, by combining data from different satellite look directions (e.g., Fialko et al., 2001b; Wright et al., 2004b; Biggs et al., 2009b; Samsonov and d'Oreye, 2012). We do not solve for N–S motion, as the satellite line of sight (LOS) is least sensitive to this component. We use stacks calculated

Table 1
Interferograms (igrams) used in this study and for stacking.

			Dataset		Stack	
Satellite	Track	Mode	Igrams	Span	Igrams	Span
ERS-1/2	70	Descending	55	Jun 1992–Sep 2000	36	Jun 1992–Sep 2000
ENVISAT	435	Ascending	82	May 2004–Aug 2010	25	Aug 2004–Aug 2010
ENVISAT	342	Descending	104	Nov 2005–Oct 2010	34	Jul 2005–Sep 2010
ALOS	163	Ascending	16	Mar 2007–Nov 2010	9	Sep 2007–Nov 2010

for ENVISAT ascending and descending tracks, each of which records displacements in a different LOS. In each case, the LOS is described by the satellite unit look vector, l, and the LOS displacements, d_{LOS}, are equal to the product of the satellite unit look vector and the vector components of displacement:

$$d_{LOS} = (-\cos\phi \sin\theta \cos\theta).\begin{pmatrix} u_E \\ u_Z \end{pmatrix}, \quad (1)$$

where θ is the look angle of the satellite at each pixel and ϕ is the heading direction of the satellite (Wright et al., 2004b). The horizontal and vertical components of motion may be calculated using $\mathbf{D} = \mathbf{Lu}$, where $\mathbf{D}$ is the LOS interferogram displacement for each dataset, and $\mathbf{L}$ is a matrix containing the look vector for each dataset. The inversion is weighted using a covariance matrix containing the mean value of σ for each dataset, which allows us to calculate the error of each displacement component (Wright et al., 2004b).

2.3. Source modeling

The results of stacking were used to carry out analytical source modeling, providing first order constraints upon the geometry and depth of the deformation source. Although these models are an oversimplification of the real earth and do not account for heterogeneities in crustal structure or rheology, they are a valuable first step in understanding the cause of subsidence (e.g., Dzurisin, 2007; Segall, 2010). Such models can be used to distinguish between shallow- and deep-seated deformation mechanisms e.g., hydrothermal system depressurisation verses magma cooling (e.g., Mann and Freymueller, 2003); and to differentiate between vertical or horizontally elongate geometries, which may be used to shed light on mechanisms of magma transport and emplacement (e.g., Bagnardi et al., 2013). This simple modeling approach also provides a useful mode of comparison with ground deformation at other volcanoes.

We use the ratio of horizontal to vertical displacements to guide source modeling as point sources (e.g., Mogi, 1958) or vertically elongate sources (e.g., prolate ellipsoids: Yang et al., 1988) generate larger horizontal displacements than horizontally elongate sources (e.g., rectangular dislocations: Okada, 1985; or penny-shaped cracks: Fialko et al., 2001a). We downsample the data to an initial resolution of ~450 m (e.g., Hamling et al., 2014), and the best-fitting source parameters are then obtained using a Monte Carlo type simulated annealing algorithm (Amelung and Bell, 2003), which provides an efficient way of testing a wide range of source parameters. We exploit the fact that we have constraints upon different components of the deformation field and simultaneously solve for all datasets. The initial range of source parameters is made broad enough to ensure that solutions do not saturate at the parameter bounds. As the source models are non-unique, we investigate the uncertainties and trade-offs between source parameters using a Monte Carlo approach (Wright et al., 2004a; Biggs et al., 2009a). This is done using covariance analysis to create 100 sets of synthetic noise, which are added to the stacks shown in Fig. 3 before rerunning the same inversion scheme.

2.4. Time-series

Finally we use time-series (e.g., Lundgren et al., 2001; Berardino et al., 2002) to assess the temporal characteristics of deformation. As measurements are made from multiple satellite tracks, we use a joint inversion technique that combines multiple sets of InSAR data (Biggs et al., 2010; Parks et al., 2015). In this approach, the observations of ground displacement are converted to incremental subsurface volume changes that arise due to point source pressure variations at depth (Mogi, 1958). The surface displacement at any point can be predicted

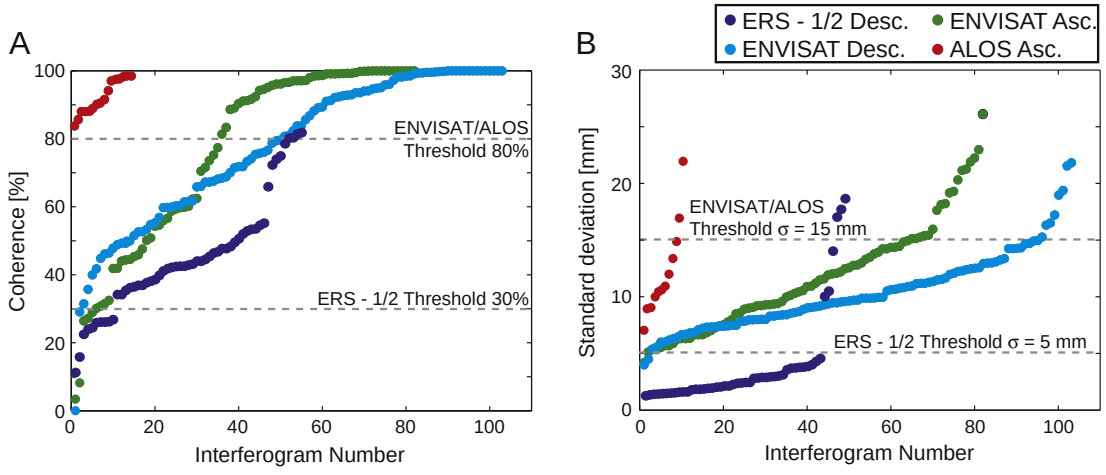

Fig. 2. A) Coherence of all interferograms listed in Table 1. Only interferograms with coherence above the labelled thresholds are used for stacking. B) Standard deviation (σ) of all interferograms listed in Table 1 calculated using covariance analysis (Hanssen, 2001). Only interferograms with σ below the labelled thresholds are used for further analysis.

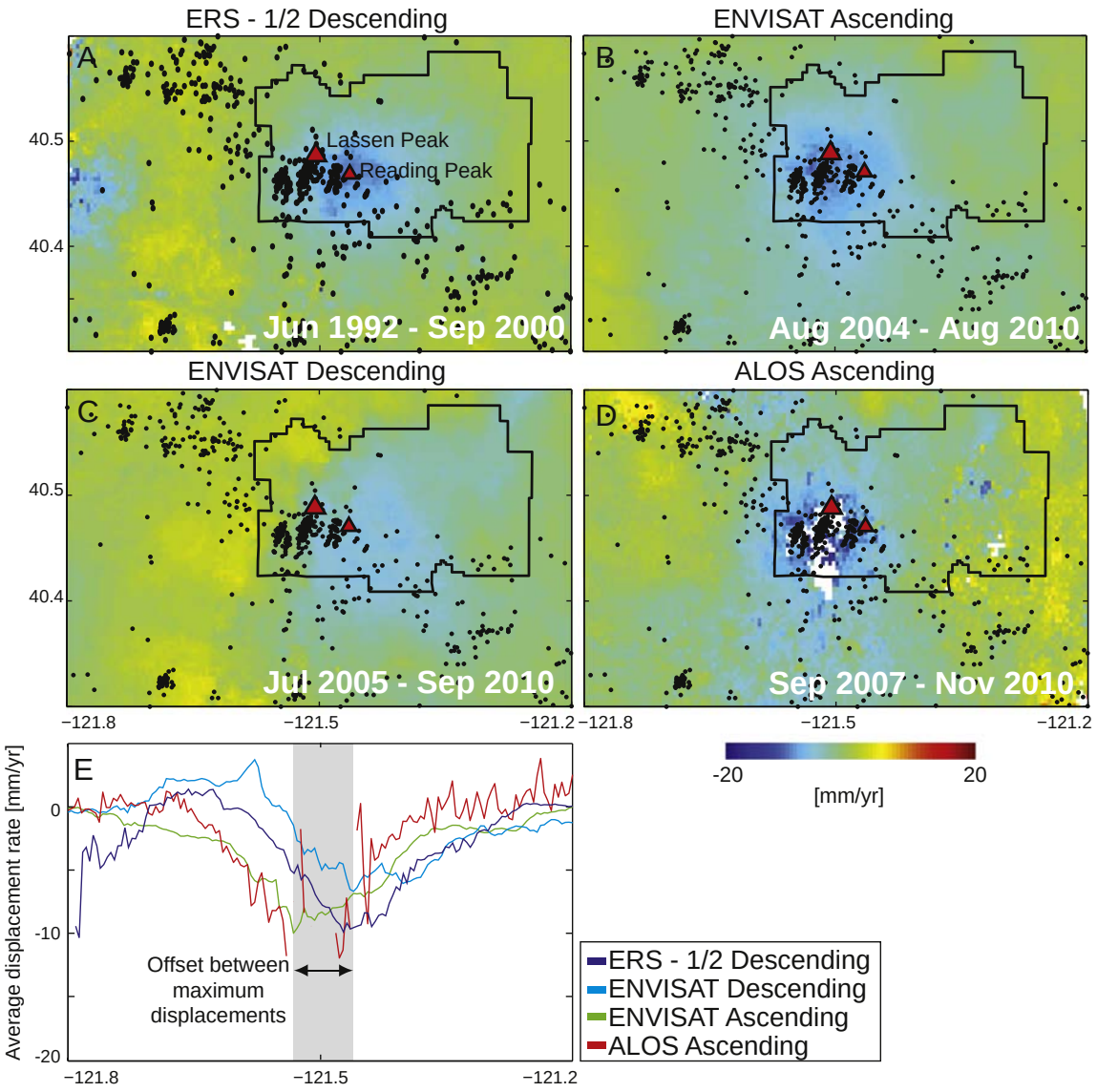

Fig. 3. A–D) Stacks for ERS-1/2 descending, ENVISAT ascending, ENVISAT descending and ALOS ascending datasets produced using the interferograms listed in Table 1. Black line shows the outline of Lassen Volcanic National Park and earthquake locations are as in Fig. 1. E) Profiles drawn at the latitude of Reading Peak show the offset between maximum subsidence between ascending and descending datasets.

by the three component LOS unit vector, l (Eq. (1)), and the three component displacement vector, M, predicted by a Mogi model (Biggs et al., 2010). For an observation point with location $[x,y,z]$, M is equal to:

$$\begin{pmatrix} m_x \\ m_y \\ m_z \end{pmatrix} = \frac{\Delta V}{\pi}(1-\nu)\begin{pmatrix} \frac{x}{R^3} \\ \frac{y}{R^3} \\ \frac{z}{R^3} \end{pmatrix}, \quad (2)$$

where ΔV is a volume change, ν is Poisson's ration (0.25), R is the distance from the point source to the observation, and b are measurements of incremental surface displacement. We can then solve for the incremental volume change of the Mogi source, V:

$$\begin{matrix} (l_a.\mathbf{M_a})A_\mathbf{a} \\ (l_b.\mathbf{M_b})A_\mathbf{b} \\ \vdots \end{matrix}\begin{pmatrix} V_{12} \\ V_{23} \\ \vdots \end{pmatrix} = \begin{matrix} \mathbf{b_a} \\ \mathbf{b_b} \\ \vdots \end{matrix} \quad (3)$$

where A is a temporal design matrix documenting the epochs used to produce each displacement observation (Biggs et al., 2010). The subscripts correspond to different InSAR datasets, each of which has a different LOS unit vector (l). The solution is integrated to account for the different duration of each time-step (Biggs et al., 2010), and the error on each volume estimate is calculated during the inversion as the sum of the weighted root mean square (RMS) residuals for individual observations (Parks et al., 2015).

3. Results

3.1. Stacking and horizontal/vertical components of displacement

Stacks show maximum LOS displacement rates of -9.6 ± 1.4 mm/yr (ERS-1/2 descending), -8.5 ± 2.4 mm/yr (ENVISAT ascending), -7.0 ± 1.8 mm/yr (ENVISAT descending) and -11 ± 5.5 mm/yr (ALOS ascending). The errors are estimated as $\sigma/\sqrt{N}$, where σ is the mean value for each dataset found in Section 2.3 (Fig. 2B) and is assumed to be uncorrelated between observations, and N is the number of observations (e.g., Parks et al., 2011).

All stacks show subsidence extending over a broad (30–40 km) region (Fig. 3A–D). In ascending track imagery subsidence is centered

on the Middle cluster of seismicity (Fig. 3B, D), whereas in descending track imagery displacements are centered on the East cluster (Fig. 3A, C). Similarly, displacement profiles taken at the latitude of Reading Peak and the longitude of Lassen Peak show that the longitude of the maximum displacement is offset by 8–10 km, whereas the latitude of the maximum displacement is the same between ascending and descending datasets (Fig. 3E). As InSAR data are acquired from a side-looking satellite platform, the eastward component of deformation is positive (towards satellite) for a descending orbit and negative (away from satellite) for an ascending orbit (e.g., Rosen et al., 2000), and this difference is therefore likely to be due to a component of east–west motion (e.g., Hooper et al., 2007).

Combining ascending and descending ENVISAT stacks using Eq. (1), we find that the maximum horizontal (eastward) displacements at LVC are ~10–15 mm/yr in magnitude, and maximum vertical displacements are ~5–10 mm/yr (Fig. 4A, B). The ratio of horizontal to vertical displacements may therefore be up to 3:1. Displacement profiles show that the maximum vertical displacements, and the change from positive to negative horizontal displacements (i.e. eastward to westward motion), occur SE of Lassen Peak at the latitude of Reading Peak (Fig. 4C, D). Whilst the vertical displacements are focussed in the vicinity of Lassen and Reading Peaks, the horizontal component of motion extends over a broader region to the N and S (Fig. 4A, B). Drawing an additional profile S of LVC (Fig. 4E, F) we observe up to ~7 mm/yr of horizontal motion. Displacements measured along the profile are in the opposite direction to tectonic extension in the region, with eastward displacements W of LVC and westward displacements E of LVC (Fig. 4E). This signal may be a result of residual atmospheric or orbital noise in the interferograms and we suggest that analysis of regional GPS is required to better quantify the magnitude of regional horizontal motion at LVC.

3.2. Best-fitting source model

Given the ratio of horizontal to vertical displacements, we model subsidence of LVC using a point source and a vertically elongate (prolate) ellipsoid. A point source is parameterized in terms of an $[x,y]$ location, depth and volume change (Mogi, 1958). An ellipsoid geometry requires an $[x,y]$ location, depth, strength term, a plunge and trend describing the inclination and orientation, and the ratio between minor and major axes, which is able to vary between 1 (for a sphere) and $\rightarrow 0$ (for a closed pipe) (Yang et al., 1988). For all model geometries, the $[x,y]$ location of the source is well constrained to be SW of Reading Peak and SE of Lassen Peak (Fig. 5A, B), which is in agreement with preliminary models presented by Poland et al. (2004) (Table 2).

Through Monte Carlo error analysis we identify a trade-off between the depth and strength of the point source model (Fig. 5C). The best-fitting point source model is located at 8.3 $\pm$0.13 depth and predicts a mean rate of volume change of -0.00286 $\pm$ 0.00012 km^3/yr between 1992 and 2010. (Note that these calculated 1σ error bounds are likely to be underestimates of the uncertainty on the model parameters.)

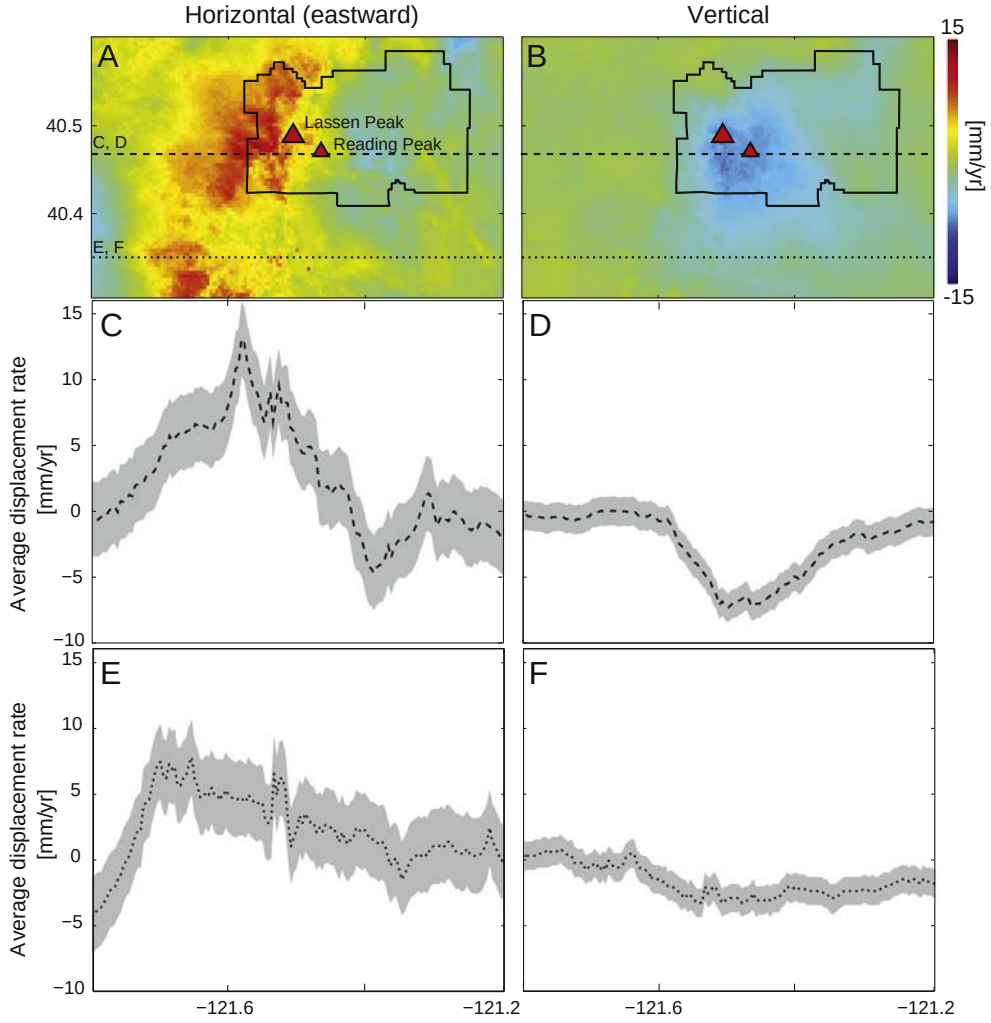

Fig. 4. A–B) Horizontal (eastward) and vertical components of motion found by combining ENVISAT ascending and descending track stacks (Fig. 3B, C). Black line shows the outline of Lassen Volcanic National Park. Dashed line marks the location of the profiles drawn in C, D, and dotted line marks the location of the profile drawn in E and F. C–F) Profiles of horizontal and vertical components of motion with 1σ errors calculated using the method described in the text. Negative eastward displacements are equivalent to westward motion.

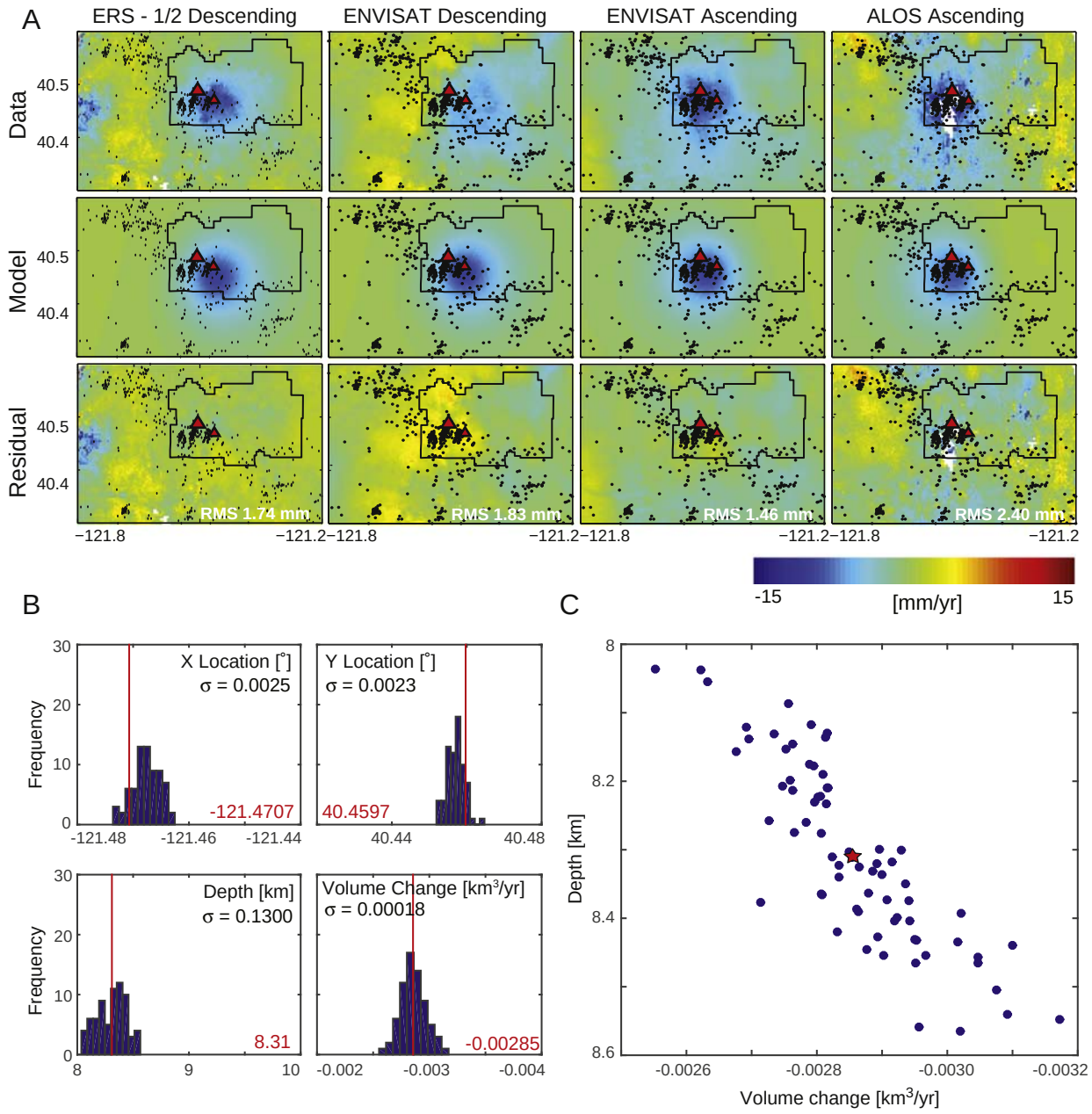

Fig. 5. Results of Mogi modeling. A) Data, model, and residuals for ERS-1/2 descending, ENVISAT descending, ENVISAT ascending and ALOS ascending datasets. Black dots show seismicity as in Fig. 1. The black line shows the outline of Lassen Volcanic National Park and the red triangles show Lassen and Reading Peak. Residual plots are labelled with RMS misfits. B) Histograms show the distribution of model parameters found via Monte Carlo analysis. Red lines and text describe the best fitting model, with 1σ values also labelled. C) Scatter plot shows the tradeoff between the rate of volume change and the source depth, with the best fitting solution marked with the red star. (For interpretation of the references to colour in this figure legend, the reader is referred to the web version of this article.)

This depth is slightly shallower than that predicted by Poland et al. (2004) (11.6 km), but is consistent with a source located in the deeper part of the magmatic system. The RMS errors for the best-fitting source geometry described in Table 2 are 1.74 mm, 1.46 mm, 1.82 mm and 2.40 mm for ERS-1/2 descending, ENVISAT ascending, ENVISAT descending and ALOS ascending datasets respectively (Fig. 5A). We test models of vertically elongate ellipsoids, but through Monte Carlo analysis find that the axis ratio term saturates at the minimum possible value and therefore, as the Mogi model provides a good fit to the data, we do not favour an ellipsoidal source geometry.

Table 2
Best-fitting analytical source models with bounds from Monte Carlo error analysis.

Source	Reference	Longitude [°]	Latitude [°]	Depth [km]	Volume change [km³/yr]
Mogi	Poland et al., 2004	−121.47	40.46	11.60	−0.0070
Mogi	This study	−121.47	40.45	8.18	−0.0027
		−121.46	40.46	8.45	−0.0030

3.3. Time-series of source volume change

We have shown that subsidence of LVC is well approximated using a point source (Fig. 5A). Using the [*x*,*y*] location and depth of the source described in Table 2, we produce a time-series of incremental source volume change for the displacements recorded by ENVISAT and ERS-

1/2 datasets. We choose to use all interferograms with σ less than the thresholds used for stacking, but time-series produced using all interferograms, or the subsets of interferograms listed in Table 1 show comparable results (Fig. S.1 in the supplementary material).

The time-series shows that between 1992 and 2000, ERS-1/2 recorded source volume change at an apparently linear rate of -0.0018 ± 0.0004 km ^{3}/yr (Fig. 6A), where the rate is calculated using a linear least squares regression and the errors are 95% confidence intervals. There is then a 4 year data gap between the last ERS-1/2 acquisition in 2000 and the first ENVISAT acquisition in 2004. In the absence of other geodetic measurements during this period, we estimate the offset between the two sections of the time-series assuming that the 1992–2000 rate continued linearly until 2004.

ENVISAT data suggest that the rate of subsidence at LVC may have varied over time (Fig. 6A). Firstly, we find that best-fitting models to individual ENVISAT interferograms tend to require larger volume changes between 2004 and 2007 than between 2007 and 2010 (see examples in Fig. 6B), and the best fitting rate of volume change during the 2004–2007 period is ~5 times larger than that for 2007–2010. However, using a segmented, rather than single linear regression, to calculate the rate of volume change between 2004 and 2010 decreases the R^2 value from 0.56 to 0.24 if we adjust for the increase in the number of degrees of freedom. We therefore prefer to use a single rate of volume change for the 2004–2010 period. The best fitting rate of volume change for all ENVISAT data between 2004 and 2010 is -0.0014 ± 0.0003 km ^{3}/yr (Fig. 6B). The error bounds on this measurement overlap with the rate obtained from ERS-1/2 between 1992 and 2000, suggesting that the rate of volume change at LVC is either constant or overall has slightly decreased relative to 1992–2000. Further extending the time-series using GPS or more recent InSAR datasets will confirm whether this is the case.

4. Discussion

4.1. Onset of subsidence

The available archive of InSAR data at LVC reveals that subsidence has been ongoing since at least 1992, but to constrain the onset of deformation we must consider evidence from earlier ground-based geodetic surveys. Leveling measurements suggest that between the 1930s and 1991 there was no deformation greater than the uncertainty in the measurements (10–20 mm: Dzurisin, 1999). However, the leveling benchmarks at LVC are located at least 10 km from the center of deformation, and the two segments of the line are orientated almost tangentially to the maximum subsidence signal located close to Reading Peak (Fig. 1A). Taking profiles across the vertical component of deformation (Fig. 4 B) that are proximal to the leveling line shows that, at the 2004–2010 rate, differential displacements recorded along the lines would be on the order of ~2 mm/yr. It is therefore possible that deformation could have been occurring for up to 10 years before being observable above the uncertainty in the leveling measurements. If subsidence had been occurring at this rate for the whole period between leveling surveys we would expect >100 mm of deformation, which is much larger than the measurement uncertainty.

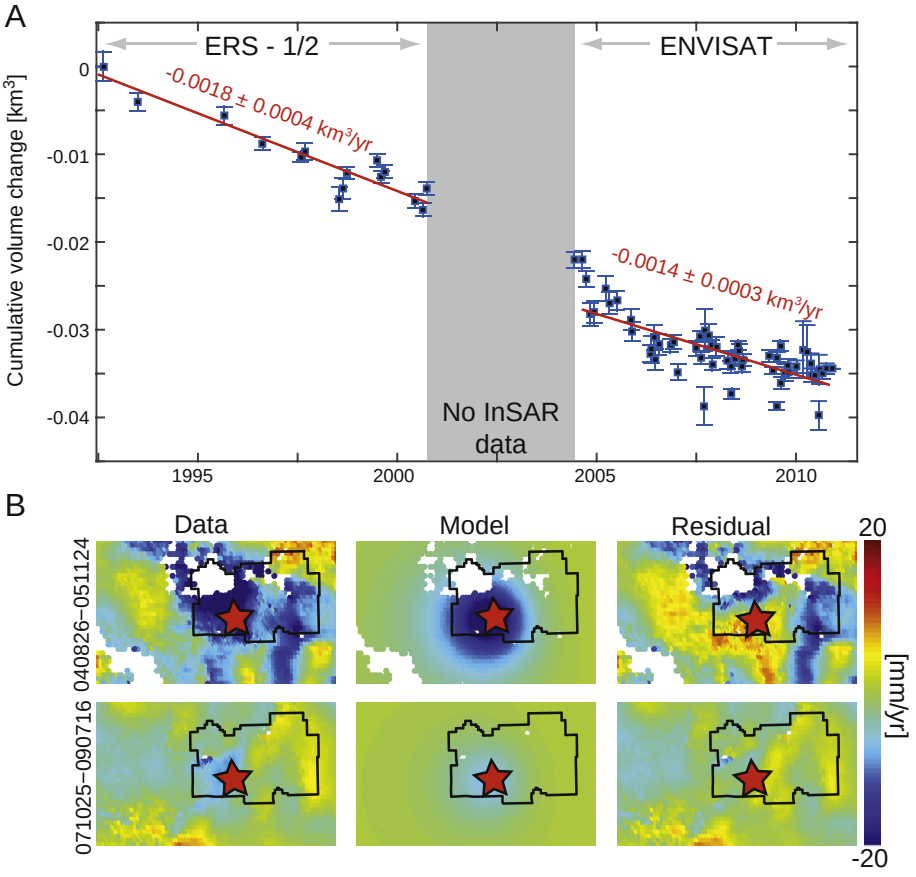

Fig. 6. A) Time-series of the rate of volume change found using ERS-1/2 and ENVISAT interferograms. Errorbars are calculated using the method described in the text. B) Examples of data, model, residuals for ENVISAT interferograms during top: 2004–2007 (possible increase in source volume loss); and bottom: 2007–2010 (subsequent period of decreased volume loss). Dates are in yymmdd–yymmdd format. The source location used in the inversion is shown by the star and described in Table 2.

Evidence from the EDM network is somewhat inconclusive. Between 1981 and 1982 Chadwick et al. (1985) found no evidence for deformation above the uncertainty in the measurements (±3.9 ppm). A net contraction of the network was then measured between 1982 and 1984. Chadwick et al. (1985) attributed this, at least in part, to windy survey conditions, but conclude that they cannot rule out the possibility of slight contraction of LVC during this period. The EDM network was most recently surveyed in 2004 using GPS, revealing line-length changes of up to 145 mm (Poland et al., 2004). Instrument inconsistencies are likely to yield large uncertainties (magnitude unspecified in Poland et al., 2004) on these measurements, however this does support evidence from ERS-1/2 that subsidence at LVC was ongoing prior to 2000.

Overall the geodetic record at LVC clearly documents subsidence since at least 1992. Whilst the leveling and EDM measurements do not allow us to constrain the onset with confidence, both datasets permit deformation to have been ongoing since the early 1980s. The absence of deformation in leveling measurements prior to this suggests it is unlikely that LVC subsided significantly during the preceding 50 years.

4.2. Comparison with Medicine Lake Volcano

Subsidence over decadal time-scales has similarly been observed at Medicine Lake Volcano, also located in the northern California portion of the Cascades Volcanic Arc. Subsidence of Medicine Lake Volcano is well characterized by geodetic measurements, including leveling surveys that began in the 1950s (Dzurisin et al., 1991; Dzurisin et al., 2002), GPS (Poland et al., 2006) and most recently InSAR (Poland et al., 2006; Parker et al., 2014). These measurements show that deformation has been occurring at a constant rate of ~10 mm/yr for over 65 years (Dzurisin et al., 2002; Poland et al., 2006; Parker et al., 2014). Whilst the magnitude of deformation is comparable to that at LVC, the temporal evolution of deformation contrasts to the InSAR measurements in this study, which suggest that the rate of volume change (and therefore subsidence) at LVC may have varied over time (Fig. 6). At Medicine Lake Volcano the vertical component of deformation is ~3 times larger than the horizontal component (Poland et al., 2006; Parker et al., 2014), whereas at LVC we find the opposite is true (Fig. 4). Consequently best fitting analytical source models at the two volcanoes are different, as measurements at Medicine Lake Volcano favour a horizontally orientated source (Poland et al., 2006; Parker et al., 2014) whereas LVC is best modeled using a point source (Table 2).

Given the comparable magnitudes of deformation and proximity within the Cascades Volcanic Arc, Poland et al. (2004) suggest that the cause of subsidence at the two volcanoes may be similar. Subsidence at Medicine Lake Volcano is thought to result from a combination of mechanisms including surface loading, combined with tectonic extension (Dzurisin et al., 2002), and cooling hot rock beneath the volcano (Poland et al., 2006). Here we evaluate whether these mechanisms may be contributing to subsidence at LVC and also consider the role of the active hydrothermal system in the measured deformation. We do not consider the small 1914–1917 eruption as a likely cause of deformation given the lack of significant subsidence between the 1930s and 1980s.

4.3. Causes of subsidence at LVC

4.3.1. Crustal extension

Both Medicine Lake Volcano and LVC are located in a region of tectonic extension, and focal mechanisms within the East, Middle and West seismic clusters at LVC are consistent with extension of the Basin and Range (Janik and McLaren, 2010). That extension is not apparent in displacement profiles drawn across the horizontal (eastward) component of displacement from InSAR (Fig. 4E) is unsurprising, as the magnitude of deformation is small (<10 mm/yr) and InSAR measurements are less sensitive to horizontal motion (e.g., Wright et al., 2004b).

Gravity surveys at LVC reveal a low anomaly at 3.5 km depth plus a broad triangular low at >12 km depth (Muffler et al., 2009). Muffler et al. (2009) speculate that this reflects a pull-apart basin in the upper-crust and low density material at depth, such as intrusive rocks or restricted volumes of partial melt. Deformable, high temperature crust that has been subject to repeated intrusions may act to localize extension, facilitating subsidence of the overlying volcanic edifice as is inferred at Medicine Lake Volcano (Dzurisin et al., 1991; Dzurisin et al., 2002). Similarly at Askja caldera, Iceland, viscoelastic material associated with the underlying extensional plate boundary is thought to play a significant role in volcanic subsidence in combination with changes in the shallow magmatic system (de Zeeuz-van Dalfsen et al., 2012). Ultimately measurements from the regional GPS network are required to quantify horizontal motion across LVC. In doing so there is scope to isolate the tectonic component of deformation and evaluate whether this may be occurring alongside other processes to explain the apparent onset of subsidence since the 1980s.

4.3.2. Cooling and crystallization

Cooling and crystallization of magmatic material has been linked to cases of volcanic subsidence that have continued over years–decades either at a constant (e.g., Aniakchak, Aleutians: Kwoun et al., 2006) or slowly decaying (e.g., Cerro Blanco, Andes: Pritchard and Simons, 2004) rate. Seismic and petrological observations at LVC provide strong evidence for a magmatic heat source (Section 1.2). This is in agreement with models of the LVC hydrothermal system, which suggest that hydrothermal features are located above hot, brittle rock, overlying residual magma (Janik and McLaren, 2010).

As magma cools a volume decrease occurs due to thermoelastic contraction (Lange, 1994) and the difference in density between the liquid and solid phases. Modeling the subsequent rate of volume change is dependent upon the local geothermal gradient, which may be elevated in the presence of partial melt, and latent heat released during crystallization. In their study at Okmok Volcano, Aleutians, Caricchi et al. (2014) also demonstrate the importance of accounting for gaseous phases when using models of cooling and crystallization to explain geodetic signals. For example as crystallization progresses, changes in the rate of subsidence may occur due to the exsolution or re-absoption of volatiles. In both of these cases uplift would be expected to precede subsidence (Caricchi et al., 2014).

We may also expect to observe uplift prior to the onset of subsidence due to the emplacement of new magma which then begins to cool (e.g., Seguam, Aleutians: Lu and Dzurisin, 2014). No observations of uplift at LVC have been made, suggesting that either any uplift that occurred in the 50 year interval between leveling surveys was cancelled out by subsidence, or that a now cooling magma body was previously in thermal equilibrium with the surrounding country rock. Alternatively the compressibility of the magma may have facilitated intrusion without causing deformation (e.g., Mastin et al., 2009; de Zeeuw-van Dalfsen et al., 2013). Further testing is required to assess the role of cooling and crystallization of subsurface magma in recent subsidence at LVC, but given the evidence for subsurface magma bodies from seismic imaging (Clynne, 1985), we suggest that this mechanism is likely to be a contributing factor.

4.3.3. Changes in the distribution of magmatic/hydrothermal fluids

Volcanic subsidence has also been linked to the migration of fluids from a magmatic (e.g., Askja, Iceland: de Zeeuw-van Dalfsen et al., 2013) or hydrothermal (e.g., Campi Flegrei, Italy: Lundgren et al., 2001; Battaglia et al., 2006) reservoir. Vent locations, lineations of seismicity (Fig. 1A), and the distribution of hydrothermal alteration all reflect lateral structural controls upon the flow of magmatic and hydrothermal fluids at LVC, as faults and other zones of enhanced permeability act as conduits to shallow depths beneath the volcano (Rose

et al., 1994). LP earthquakes also provide evidence of the movement of magma/fluids at depth, although at LVC these events are located further W of the modeled source location and the West cluster of seismicity (Pitt et al., 2002), (Fig. 1A).

The downward drainage of magmatic fluid may be expected to cause an increase in source depth over time. For a Mogi-type source an increasing source depth may not be distinguishable from a decrease in the rate of volume change due to the trade-off between these model parameters (e.g., Fig. 5C). The InSAR data at LVC are therefore conducive to a deepening source but do not permit a rigorous assessment of this hypothesis. Similarly the depth of the subsidence source inferred from analytical models (~8 km), which is greater than the depth of the hydrothermal system (5 km: Ingebritsen et al., 2016), may be biased by the effects of broader, regional scale deformation associated with extension (e.g., Askja: de Zeeuz-van Dalfsen et al., 2012). Interestingly, the possible increase in the rate of volume loss identified in the time-series between 2004 and 2007 (Fig. 6A) is coincident with an increase in recorded seismicity in the East, Middle and West clusters, all of which are linked to the hydrothermal system (Janik and McLaren, 2010). However, this increase in seismicity during the early 2000s may be due, in part, to greater scrutiny of the seismic record (Janik and McLaren, 2010), and given the current modeled depth of the source, any link between the two is speculative.

One possible trigger of changes in the distribution of fluids that would explain possible quiesence prior to the onset of subsidence is regional seismic activity. This is thought to have caused subsidence at hydrothermally active, previously non-deforming volcanoes in Japan and South America (Takada and Fukushima, 2013; Pritchard et al., 2013). In 1992 the M_w 7.3 Landers earthquake, located 840 km SSE of LVC, triggered 38 seismic events at LVC including a M_w 3.5 event within 13 min of the mainshock (Hill et al., 1993; McLaren and Janik, 1996). Whilst the geodetic record is permissive of deformation commencing at the time of this event, in both South America and Japan ground displacements were 5–15 cm in magnitude, occurring within days (e.g., Azuma, Japan: Takada and Fukushima, 2013) to weeks (e.g., Caldera del Atuel, Chile: Pritchard et al., 2013) after the earthquake. This is at odds with the long-term rate of subsidence observed at LVC, and at this stage it is difficult to envisage why deformation following the Landers earthquake would continue for decades.

5. Conclusions

Lassen Volcanic Center is one of only two Cascade volcanoes to have erupted in the 20th century, but is one of four Cascade volcanoes to have exhibited subsidence during the same time period (others are Medicine Lake Volcano: Dzurisin et al., 1991; Mount Baker: Hodge and Crider, 2010; and Mount St Helens: Poland and Lu, 2008). Whilst not immediately linked to eruption hazards, volcanic subsidence is a frequently observed yet poorly understood phenomenon, and can be used to provide insight into magma storage conditions, plus other long-term processes related to tectonic setting and evolving hydrothermal systems. Here we have used the archive of InSAR data to add to examples of known volcanic subsidence and better understand the temporal and spatial characteristics of deformation at LVC. These measurements reveal that on the order of 10 mm/yr of subsidence was ongoing between 1992 and 2010, and that the rate of subsurface volume loss may have varied over time. Whilst the magnitude of deformation is comparable to that at neighboring Medicine Lake Volcano, the ratio of horizontal to vertical displacements is quite different, favoring a point source located at ~8 km depth, rather than horizontally orientated source. Key to understanding ongoing subsidence at these and other volcanoes is an assessment of the interaction between volcanic and tectonic causes of deformation. At LVC we suggest that regional GPS measurements will provide improved constraints upon the contribution of tectonic extension to subsidence, allowing a more thorough evaluation of the role of the hydrothermal and magmatic systems in ground deformation over recent decades.

Supplementary data to this article can be found online at http://dx.doi.org/10.1016/j.jvolgeores.2016.04.013.

Acknowledgements

This research was carried out as part of an Open CASE Natural Environmental Research Council PhD studentship in conjunction with the U.S. Geological Survey Cascades Volcano Observatory. J. Biggs was also supported by Natural Environmental Research Council funding through COMET. SAR data was obtained via the Alaska SAR Facility and the WInSAR consortium. An earlier version of manuscript was greatly improved by comments and insights from reviewers M. Poland and M. Clynne.

References

Amelung, F., Bell, J., 2003. Interferometric synthetic aperture radar observations of the 1994 Double Spring Flat, Nevada, earthquake (M5.9): main shock accompanied by triggered slip on a conjugate fault. J. Geophys. Res. 108 (B9).
Bagnardi, M., Amelung, F., Poland, M.P., 2013. A new model for the growth of basaltic shields based on deformation of Fernandina volcano, Galápagos Islands. Earth Planet. Sci. Lett. 377, 358–366.
Battaglia, M., Troise, C., Obrizzo, F., Pingue, F., De Natale, G., 2006. Evidence for fluid migration as the source of deformation at Campi Flegrei caldera (Italy). Geophys. Res. Lett. 33 (1).
Berardino, P., Fornaro, G., Lanari, R., Sansosti, E., 2002. A new algorithm for surface deformation monitoring based on small baseline differential SAR interferograms. IEEE Trans. Geosci. Remote Sens. 40, 2375–2383.
Biggs, J., Wright, T., Lu, Z., Parsons, P., 2007. Multi-interferogram method for measuring inter seismic deformation: Denali Fault, Alaska. Geophys. J. Int. 170, 1165–1179.
Biggs, J., Anthony, E.Y., Ebinger, C.J., 2009a. Multiple inflation and deflation events at Kenyan volcanoes, East African rift. Geology 37 (11), 979–982.
Biggs, J., Robinson, D.P., Dixon, T.H., 2009b. The 2007 Pisco, Peru, earthquake (M8.0): seismology and geodesy. Geophys. J. Int. 176, 657–669.
Biggs, J., Lu, Z., Fournier, T., Freymueller, J.T., 2010. Magma flux at Okmok Volcano, Alaska, from a joint inversion of continuous GPS, campaign GPS and interferometric synthetic aperture radar. J. Geophys. Res. 115 (B12401).
Biggs, J., Ebmeier, S.K., Aspinall, W.P., Lu, Z., Pritchard, M.E., Sparks, R.S.J., Mather, T.A., 2014. Global link between deformation and volcanic eruption quantified by satellite imagery. Nat. Commun. 5.
Blakeslee, M.W., Kattenhorn, S.A., 2013. Revised earthquake hazard of the Hat Creek fault, northern California: a case example of a normal fault dissecting variable-age basaltic lavas. Geosphere 9 (5), 1397–1409.
Caricchi, L., Biggs, J., Annen, C., Ebmeier, S., 2014. The influence of cooling, crystallisation and re-melting on the interpretation of geodetic signals in volcanic systems. Earth Planet. Sci. Lett. 388, 166–174.
Chadwick, W.W., Iwatsubo, E.Y., Swanson, D.A., Ewert, J.W., 1985. Measurements of slope distances and vertical angles at Mount Baker and Mount Rainier, Washington, Mount Hood and Crater Lake, Oregon, and Mount Shasta and Lassen Peak, California, 1980–1984. U.S. Geol. Surv. Open File Rep. 85–205.
Chiodini, G., Vandemeulebrouck, J., Caliro, S., D'Auria, L., De Martino, P., Mangiacapra, A., Petrillo, Z., 2015. Evidence of thermal-driven processes triggering the 2005–2014 unrest at Campi Flegrei caldera. Earth Planet. Sci. Lett. 414, 58–67.
Clynne, M.A., 1985. Quaternary volcanism in the southernmost Cascade Range, California.
Clynne, M. A., Muffler, L. J. P., 2010. Geologic map of Lassen Volcanic National Park and vicinity, California. I - 2899, scale 1:50,000, 110.
Clynne, M.A., Robinson, J.E., Nathenson, M., Muffler, L.J.P., 2012. Volcano hazards assessment for the Lassen region, Northern California. U. S. Geol. Surv. Sci. Investig. Rep. (2012–5176-A, 56 p).
de Zeeuw-van Dalfsen, E., Rymer, H., Sturkell, E., Pedersen, R., Hooper, A., Sigmundsson, F., Ófeigsson, B., 2013. Geodetic data shed light on ongoing caldera subsidence at Askja, Iceland. Bull. Volcanol. 75 (5), 1–13.
de Zeeuz-van Dalfsen, E., Pedersen, R., Hooper, A., Sigmundsson, F., 2012. Subsidence of Askja caldera 2000–2009: modelling of deformation processes at an extensional plate boundary constrained by time series InSAR analysis. J. Volcanol. Geotherm. Res. 213, 72–82.
Donnelly-Nolan, J.M., Grove, T.L., Lanphere, M.A., Champion, D.E., 2008. Eruptive history and tectonic setting of Medicine Lake Volcano, a large rear-arc volcano in the southern cascades. J. Volcanol. Geotherm. Res. 117 (2), 313–328.
Dzurisin, D., 1999. Results of repeated leveling surveys at Newberry Volcano, Oregon, and near Lassen Peak Volcano, California. Bull. Volcanol. 61 (1–2), 83–91.
Dzurisin, D., 2007. Volcano Deformation: Geodetic Monitoring Techniques. Springer-Praxis, Chichester, UK.
Dzurisin, D., Donnelly-Nolan, J.M., Evans, J.R., Walter, S.R., 1991. Crustal subsidence, seismicity, and structure near Medicine Lake Volcano, California. J. Geophys. Res. 96 (B10), 16319–16333.
Dzurisin, D., Poland, M.P., Bürgmann, R., 2002. Steady subsidence of Medicine Lake Volcano, Northern California, revealed by repeated levelling surveys. J. Geophys. Res. 107 (B12) (ECV 8–1–ECV 8–16).

Fialko, Y., Khazan, Y., Simons, M., 2001a. Deformation due to a pressurised horizontal circular crack in an elastic half-space, with applications to volcano geodesy. Geophys. J. Int. 146 (1), 181–190.
Fialko, Y., Simons, M., Agnew, D., 2001b. The complete (3-D) surface displacement field in the epicentral area of the 1999 Mw 7.1 Hector Mine earthquake, California, from space geodetic observations. Geophys. Res. Lett. 28 (16), 3063–3066.
Goldstein, R., Werner, C., 1998. Radar interferogram filtering for geophysical applications. Geophys. Res. Lett. 25 (21), 4035–4038.
Goldstein, R., Zebker, H., Werner, C., 1988. Satellite radar interferometry: two dimensional phase unwrapping. Radio Sci. 23 (4), 713–720.
Gourmelen, N., Amelung, F., Lanari, R., 2010. Interferometric synthetic aperture radar-GPS integration: interseismic strain accumulation across the Hunter Mountain fault in the eastern California shear zone. J. Geophys. Res. 115 (B9).
Hamling, I.J., Wright, T.J., Calais, E., Lewi, E., Fukahata, Y., 2014. InSAR observations of post-rifting deformation around the Dabbahu rift segment, Afar, Ethiopia. Geophys. J. Int. 197 (1), 33–49.
Hanssen, R.F., 2001. Radar Interferometry: Data Interpretation and Analysis. Kluwer Acad, Norwell, MA, US.
Hildreth, W., 2007. Quaternary magmatism in the cascades — geological perspectives. U.S. Geol. Surv. Prof. Pap. 1744, 125.
Hill, D.P., Reasenberg, P.A., Michael, A., Arabaz, W.J., Beroza, G., Brumbaugh, D., Brune, J.N., Castro, R., Davis, S., Ellsworth, W.L., et al., 1993. Seismicity remotely triggered by the magnitude 7.3 Landers, California, earthquake. Science 260 (5114), 1617–1623.
Hodge, B.E., Crider, J.G., 2010. Investigating mechanisms of edifice deflation 1981–2007, at Mount Baker volcano, Washington, United States. J. Geophys. Res. 105, 25671–25684.
Hooper, A., Segall, P., Zebker, H., 2007. Persistent scatterer interferometric synthetic aperture radar for crustal deformation analysis, with application to Volcán Alcedo, Galápagos. J. Geophys. Res. 112 (B7).
Humphrey, J., McLaren, M., 1995. Seismicity along the boundary between the Modoc Plateau, southern Cascade Mountains, and northern Sierra Nevada Previously was In: Page, W.D. (Ed.), Quaternary Geology Along the Boundary Between the Modoc Plateau, Southern Cascade Mountains and Northern Sierra Nevada. Friends of the Pleistocene, 1995 Pacific Cell Field Trip, Appendix A 27.
Ingebritsen, S.E., Shelly, D.R., Hsieh, P.A., Clor, L.E., Seward, P.H., Evans, W.C., 2015. Hydrothermal response to a volcano-tectonic earthquake swarm, Lassen, California. Geophys. Res. Lett. 42 (21), 9223–9230.
Ingebritsen, S.E., Bergfeld, D., Clor, L.E., Evan, S., William, C., 2016. The Lassen hydrothermal system. Am. Mineral. 101 (2), 343–354.
Janik, C.J., McLaren, M.K., 2010. Seismicity and fluid geochemistry at Lassen Volcanic National Park, California: evidence for two circulation cells in the hydrothermal system. J. Volcanol. Geotherm. Res. 189 (3), 257–277.
Jónsson, S., Zebker, H., Segall, P., Amelung, F., 2002. Fault slip distribution of the 1999 Mw 7.1 Hector Mine, California, earthquake, estimated from satellite radar and GPS measurements. Bull. Seismol. Soc. Am. 92 (4), 1377–1389.
Klein, F.W., 1979. Earthquakes in Lassen Volcanic National Park, California. Bull. Seismol. Soc. Am. 69 (3), 867–875.
Klemetti, E.W., Clynne, M.A., 2014. Localized rejuvenation of a crystal mush recorded in zircon temporal and compositional variation at the Lassen Volcanic Center, Northern California. PLoS One 9 (12), e113157.
Kwoun, O., Lu, Z., Neal, C., Wicks, C., 2006. Quiescent deformation of the Aniakchak caldera, Alaska, mapped by InSAR. Geology 34 (1), 5–8.
Lange, R.A., 1994. The effect of H_2O, CO_2 and F on the density and viscosity of silicate melts. Volatiles in Magmas. Rev. Mineral. 30, pp. 331–369.
Lu, Z., Dzurisin, D., 2014. InSAR Imaging of Aleutian Volcanoes: Monitoring a Volcanic Arc from Space. Springer-Praxis, Chichester, UK.
Lu, Z., Mann, D., Freymueller, J., 1998. Satellite radar interferometry measures deformation at Okmok Volcano. Eos. Trans. AGU 79 (39), 461–468.
Lundgren, P., Usai, S., Sansosti, E., Lanari, R., Tesauro, M., Fornaro, G., Berardino, P., 2001. Modeling surface deformation observed with synthetic aperture radar interferometry at Campi Flegrei caldera. J. Geophys. Res. 106 (B9), 19355–19366.
Mann, D., Freymueller, J., 2003. Volcanic and tectonic deformation on Unimak Island in the Aleutian arc, Alaska. J. Geophys. Res. 108 (B2).
Mastin, L., Lisowski, M., Roeloffs, E., Beeler, N., 2009. Improved constraints on the estimated size and volatile content of the Mount St. Helens magma system from the 2004–2008 history of dome growth and deformation. Geophys. Res. Lett. 36, L20304.
McLaren, M.K., Janik, C.J., 1996. Microearthquake clusters and the Lassen hydrothermal system, northern California. Eos. Trans. AGU 77, F513.
Mogi, K., 1958. Relations between eruptions of various volcanoes and the deformations of the ground surfaces around them. Bull. Earthq. Res. Inst., Univ. Tokyo 36, 99–134.
Muffler, L.J.P., Blakley, R.J., Clynne, M.A., 2009. Cascade Arc and Walker Lane interaction in the Lassen volcanic region, California (abstract). Geol. Soc. Am. Abstr. Programs 41 (7), 64.
Norris, R.D., Meagher, K.L., Weaver, C.S., 1997. The 1936, 1945–1947, and 1950 earthquake sequences near Lassen Peak, California. J. Geophys. Res. 102 (B1), 449–457.
Okada, Y., 1985. Surface deformation due to shear and tensile faults in a half-space. Bull. Seismol. Soc. Am. 75 (4), 1135–1154.
Parker, A.L., Biggs, J., Lu, Z., 2014. Investigating long-term subsidence at Medicine Lake volcano, CA, using multi temporal InSAR. Geophys. J. Int. 199 (2), 844–859.
Parker, A.L., Biggs, J., Walters, R.J., Ebmeier, S.K., Wright, T.J., Teanby, N.A., Lu, Z., 2015. Systematic assessment of atmospheric uncertainties for InSAR data at volcanic arcs using large-scale atmospheric models: application to the Cascade volcanoes, United States. Remote Sens. Environ. 170, 102–114.
Parks, M.M., Biggs, J., Mather, T.A., Pyle, D.M., Amelung, F., Monsalve, M.L., Narváez Medina, L., 2011. Co-eruptive subsidence at Galeras identified during an InSAR survey of Colombian volcanoes (2006–2009). J. Volcanol. Geotherm. Res. 202 (3), 228–240.
Parks, M.M., Moore, J., Papanikolaou, X., Biggs, J., Mather, T.A., Pyle, D.M., Raptakis, C., Paradissis, D., Hooper, A., Parsons, B., Nomikou, P., 2015. From quiescence to unrest—20 years of satellite geodetic measurements at Santorini volcano, Greece. J. Geophys. Res. 120 (2), 1309–1328.
Pearse, J., Fialko, Y., 2010. Mechanics of active magmatic intraplating in the Rio Grande rift near Socorro, New Mexico. J. Geophys. Res. 115 (B7).
Pinel, V., Poland, M.P., Hooper, A., 2014. Volcanology: lessons learned from synthetic aperture radar imagery. J. Volcanol. Geotherm. Res. 289, 81–113.
Pitt, A.M., Hill, D.P., Walter, S.W., Johnson, M.J.S., 2002. Midcrustal, long-period earthquakes beneath northern california volcanic areas. Seismol. Res. Lett. 73 (2), 144–152.
Poland, M.P., Lu, Z., 2008. Radar Interferometry observations of surface displacements during pre- and coeruptive periods at Mount St. Helens, Washington, 1992–2005. U. S. Geol. Surv. Prof. Pap. 1750, 361–382.
Poland, M., Bawden, G., Lisowski, M., Dzurisin, D., 2004. Newly discovered subsidence at Lassen Peak, southern Cascade Range, California, from InSAR and GPS. EOS Trans. Am. Geophys. Union Fall Meet. Suppl. 85 (abs. G51 A-0068).
Poland, M.P., Bürgmann, R., Dzurisin, D., Lisowski, M., Masterlark, T., Owen, S., Fink, J., 2006. Constraints on the mechanism of long-term, steady subsidence at Medicine Lake volcano, northern California, from GPS, levelling and InSAR. J. Volcanol. Geotherm. Res. 150 (1), 55–78.
Pritchard, M.E., Simons, M., 2004. Surveying volcanic arcs with satellite radar interferometry: the central Andes, Kamchatka, and beyond. GSA Today 14 (8).
Pritchard, M.E., Jay, J.A., Aron, F., Henderson, S.T., Lara, L.E., 2013. Subsidence at southern Andes volcanoes induced by the 2010 Maule, Chile earthquake. Nat. Geosci. 6 (8), 632–636.
Quinn, E.T., 2014. Experimental Determination of Pre-eruptive Storage Conditions and Continuous Decompression of Rhyodacite Magma Erupted from Chaos Crags, Lassen Volcanic Center, California (Masters Thesis) Humboldt State University.
Rose, T.P., Criss, R.E., Mughannam, A.J., Clynne, M.A., 1994. Oxygen isotope evidence for hydrothermal alteration within a Quaternary stratovolcano, Lassen volcanic National Park, California. J. Geophys. Res. 99 (B11), 21621–21633.
Rosen, P.A., Hensley, S., Joughin, I.R., Li, F.K., Madsen, S.N., Rodriguez, E., Goldstein, R.M., 2000. Synthetic aperture radar interferometry. Proc. Inst. Electron. Electr. Eng. 88 (3), 333–382.
Rosen, P., Hensley, S., Peltzer, G., Simons, M., 2004. Updated repeat orbit interferometry package released. Eos. Trans. AGU 85 (5), 47.
Samsonov, S., d'Oreye, N., 2012. Multidimensional time-series analysis of ground deformation from multiple InSAR data sets applied to Virunga volcanic province. Geophys. J. Int. 191 (3), 1095–1108.
Segall, P., 2010. Earthquake and Volcano Deformation. Princeton University Press, Princeton, New Jersey, US.
Takada, Y., Fukushima, Y., 2013. Volcanic subsidence triggered by the 2011 Tohoku earthquake in Japan. Nat. Geosci. 6 (8), 637–641.
Walter, S., Rojas, V., Kollman, A., 1984. Seismicity of the Lassen Peak area, California. Geotherm. Resour. Counc. Trans. 8, 523–527.
Wells, R.E., Weaver, C.S., Blakely, R.J., 1998. Fore-arc migration in Cascadia and its neotectonic significance. Geology 26 (8), 759–762.
Wright, T., Lu, Z., Wicks, C., 2004a. Constraining the slip distribution and fault geometry of the Mw 7.9, 3 November 2002, Denali Fault earthquake with interferometric synthetic aperture radar and global positioning system data. Bull. Seismol. Soc. Am. 94 (6B), S175–S189.
Wright, T.J., Parsons, B.E., Lu, Z., 2004b. Toward mapping surface deformation in three dimensions using InSAR. Geophys. Res. Lett. 31 (1).
Yang, X.-M., Davis, P.M., Dieterich, J.H., 1988. Deformation from inflation of a dipping finite prolate spheroid in an elastic half-space as a model for volcanic stressing. J. Geophys. Res. 93 (B5), 4249–4257.